Supplemental material to "Batchelor, Saffman, and Kazantsev spectra in galactic small-scale dynamos"

A. Brandenburg, H. Zhou, & R. Sharma

October 24, 2022, Revision: 1.12

In this Supplemental Material (SM), we present diagnostic material that was not yet included in the main paper or the appendix. These include images and spectra of the rotation measure (RM) and the E and B polarizations for synchrotron and dust emission for Runs A–E.

1 Summary of figures in SM and the paper

In Table 1, we present an overview of the figure numbers for each diagnostic item in the paper and the present SM. We recall that for Run C, only the kinematic stage was calculated.

Table 1: Figure numbers in the paper and the SM of images, spectra, and PDFs of synchrotron and dust polarizations. Except for Run C, the saturated case is given in the second row.

	Images		Spectra		
Run	sync	dust	sync	dust	PDFs
A	S1	S3	11	S5	17
	S2	S4	B3	S6	17
B	S7		B1		S10
	S8		S9		S10
C	S11		B2	—	—
D	12	14	13	15	18
	S14	S13	S12		18
E	9	S15	10	S17	16
	B4	S16	B5	S18	16

2 Results for Run A

For Run A, we only presented spectra for the kinetic case in Fig. 11 and for the saturated case in Fig. B3. Here we also present the synchrotron images for the kinematic and saturated cases in Figs. 1 and 2. In Figs. 3 and 4 we present corresponding images for dust emission for the kinematic and saturated cases.

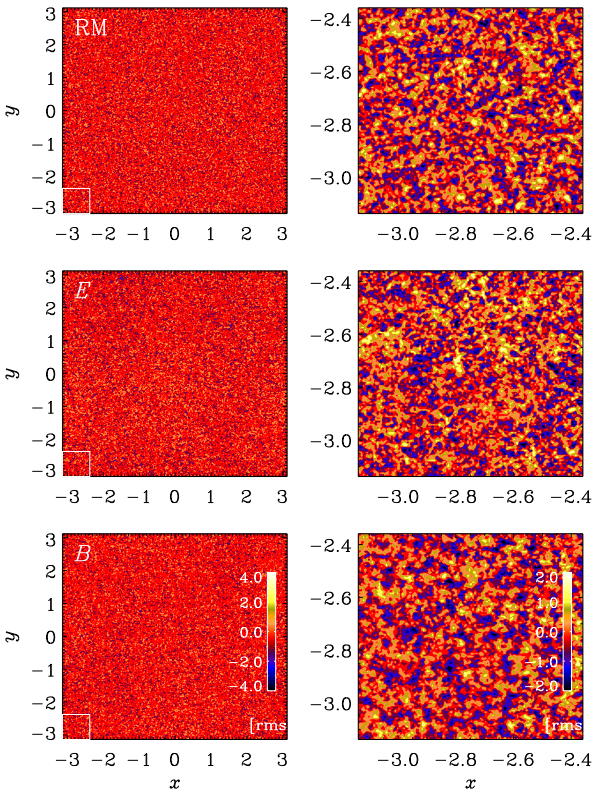

Figure 1: Synchrotron images for Run A (kinematic).

Spectra for dust emission in the kinematic and saturated stages are shown in Figs. 5 and 6.

Run A has the largest value of $k_{\rm f}/k_1$ and has therefore the smallest scale field of all runs. In the saturated stage, the B polarization shows stripes that are inclined by 45°.

For Run A, the dust polarization images are similar to the synchrotron polarization images. In particular, the stripes in the B polarization for the saturated stage are also present in the dust images.

For Run A, the dust polarization spectra are very similar to those for synchrotron emission; see Figs. 5 and 6 and compare with Figs.11 and B3 of the paper.

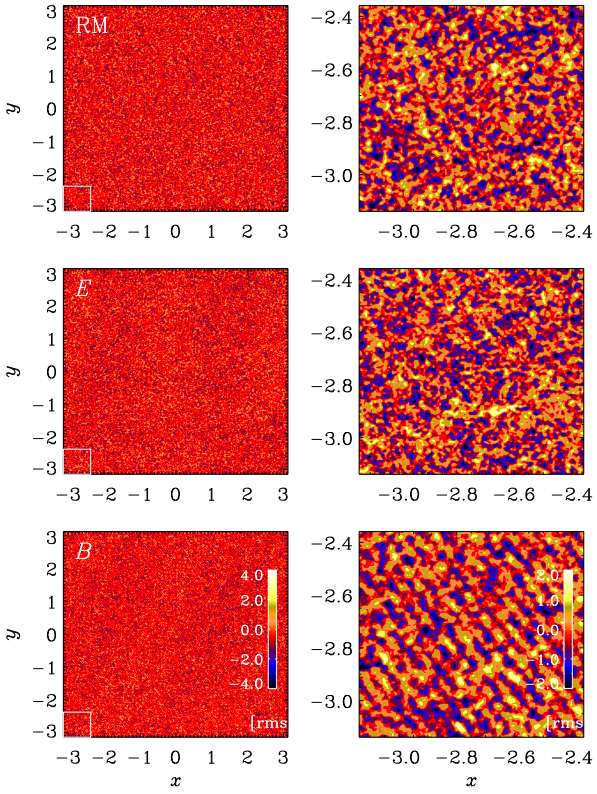

Figure 2: Synchrotron images for Run A (saturated).

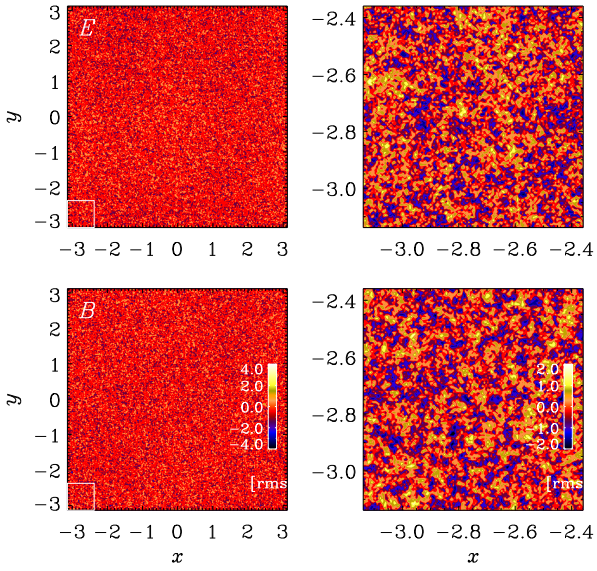

Figure 3: Dust images for Run A (kinematic).

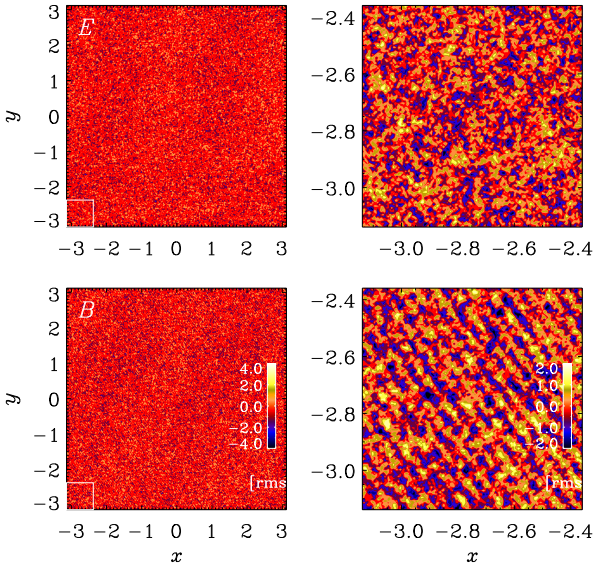

Figure 4: Dust images for Run A (saturated).

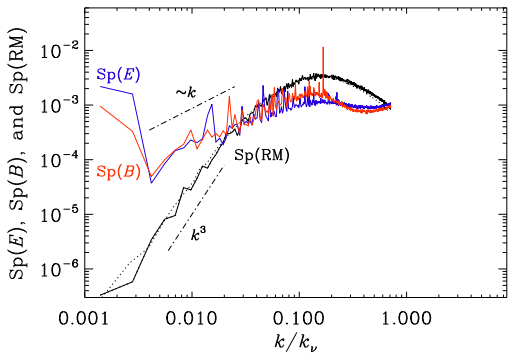

Figure 5: Dust spectra for Run A (kinematic).

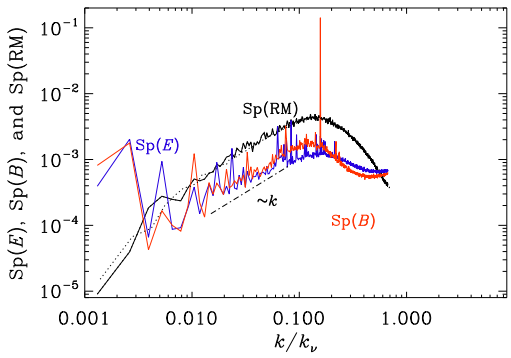

Figure 6: Dust spectra for Run A (saturated).

3 Results for Run B

For Run B, we presented synchrotron spectra for the kinematic stage in Fig. B1 of the appendix of the paper. In Figs. 7 and 8 we also present images of synchrotron in the kinematic and saturated stages. The elongated structures in the E polarization have become somewhat weaker compared to the kinematic stage.

One also notices that the structures in the B po-

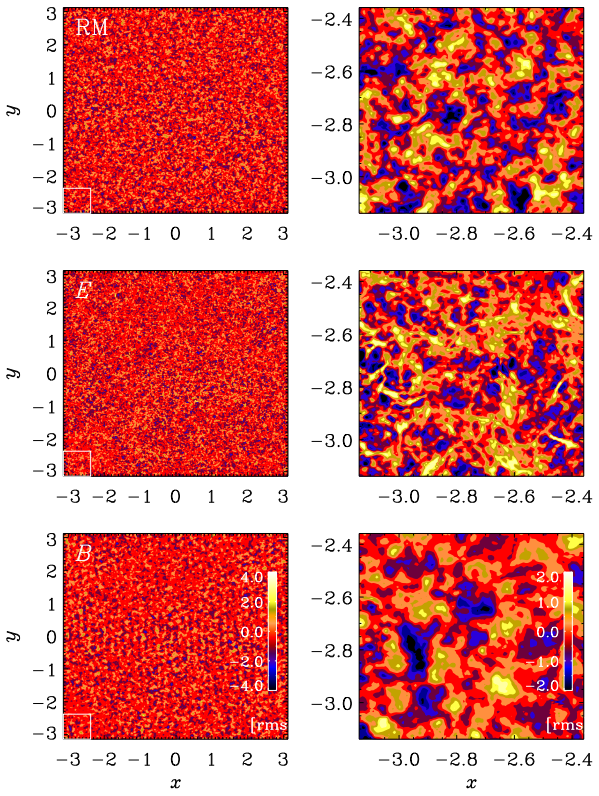

Figure 7: Synchrotron spectra for Run B (kinematic).

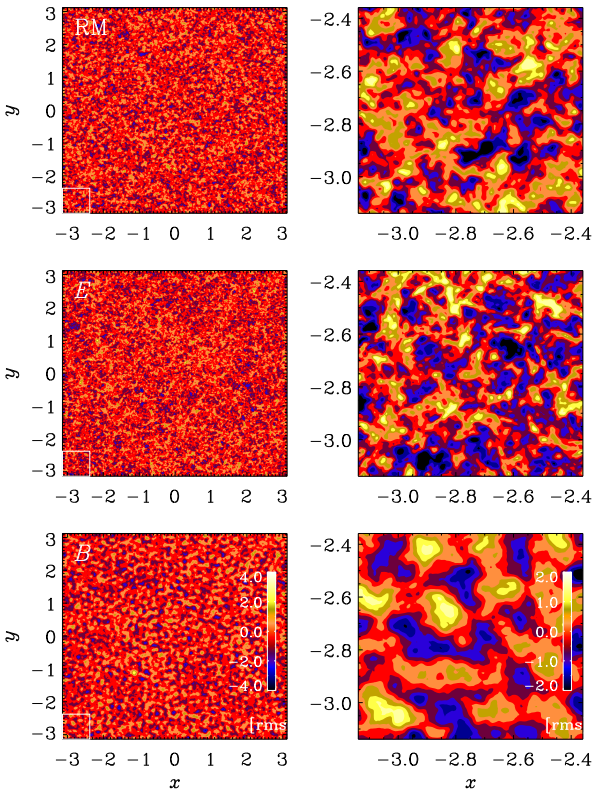

Figure 8: Synchrotron images for Run B (saturated).

larization are generally larger than for the E polarization. This is also seen in the spectra in Fig. 9, where Sp(B) is seen to decline at large k more rapidly than Sp(E). This is mostly caused by the spike in Sp(B) at the forcing scale, which gives the overall image a smoother appearance.

Run B had a scale separation of 30 ($k_{\rm f}/k_1 = 30$), a magnetic Prandtl number of unity and a Reynolds number of 81. It showed a k^3 subinertial range, which is expected to become a k^4 subinertial range in a larger domain.

The probability density functions (PDFs) of E and B show some some systematic differences in that E shows positive skewness and excess kurtosis when the magnetic Reynolds and Prandtl numbers are large. One sees this trend already for Run B; see Fig. 10. The skewness of the E polarization of Run B is slightly weaker than that of Run D shown in Fig. 16 of the paper.

4 Results for Run C

For Run C, for which we have simulated only the kinematic phase, we show in Fig. 11 images of synchrotron emission. We see that the elongated structures in the E polarization are clearly noticeable.

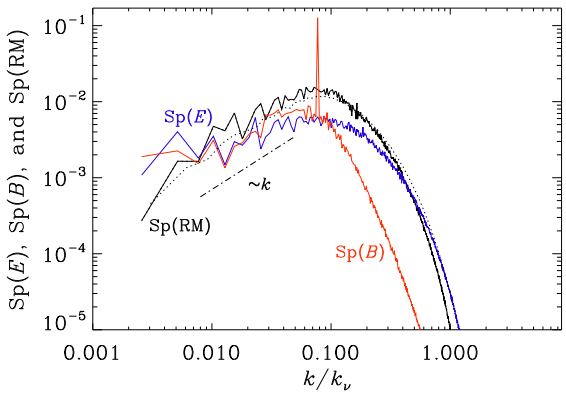

Figure 9: Synchrotron spectra for Run B (saturated).

5 Results for Run D

Run D has the largest magnetic Prandtl number of our five runs. It also has the most pronounced elongated structures in the E polarization. In the saturated state, the spectra of RM, E, and B in Fig. 12 are similar to those in the kinematic regime in Fig. 13 of the paper. The spectra are also similar to those of Run E; see Fig. B5 of the paper.

In the dust images of E, as already shown in

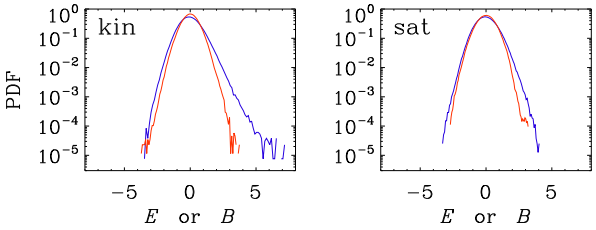

Figure 10: PDFs of E (blue lines) and B (red lines) during the kinematic (left) and saturated (right) stages for Run B.

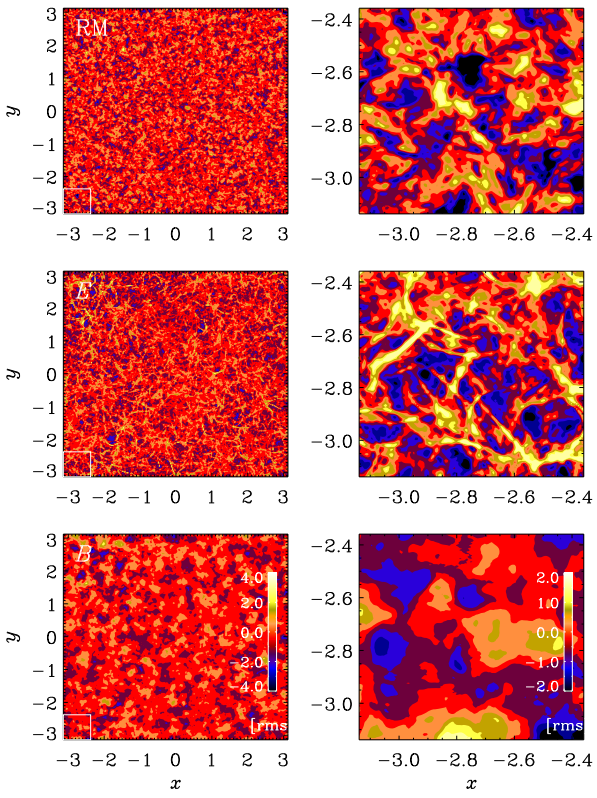

Figure 11: Synchrotron images for Run C (kinematic).

Fig. 14 of the paper, the elongated structures are absent. That is true both of the kinematic stage shown in the paper and also of the saturated state; see Fig. 13.

In the saturated state, the large-scale elongated structures in the E polarization are still present; see Fig. 14. However, the structures are now bigger and can best be seen in the full images on the left and not so well in the enlargements on the right. This is also similar to Run E; see Fig. B5 of the paper.

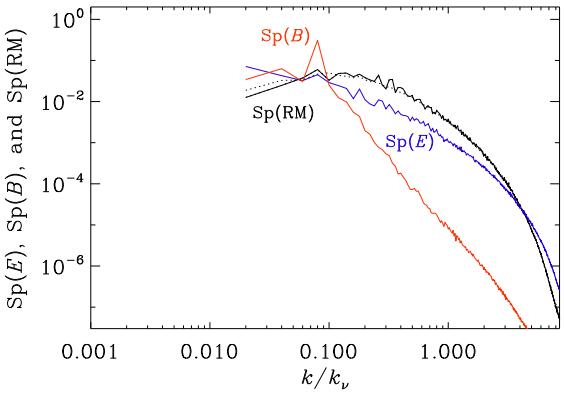

Figure 12: Synchrotron spectra for Run D (saturated).

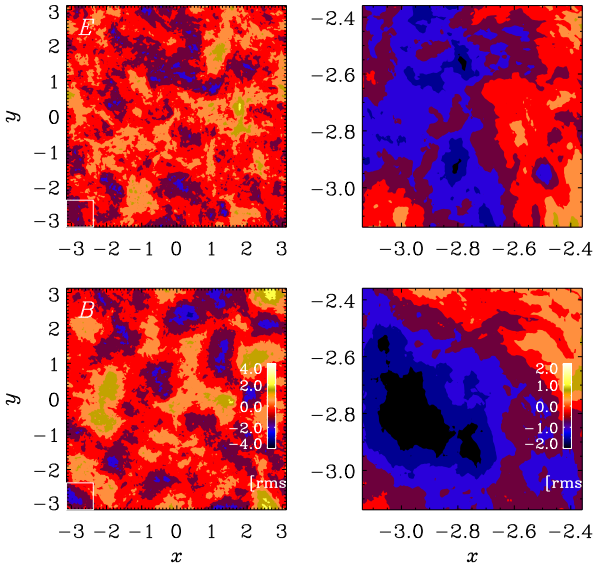

Figure 13: Dust images for Run D (saturated).

6 Results for Run E

The dust images of E and B show no elongated structures, but there are again clear differences in the typical scales of E and B, with the latter being again of larger scale. This is clearly caused by the spectral peak of B begin at the forcing scale, while that of E is at the resistive scale; see Fig. 15 for the kinematic stage. In the saturated stage, the structures are significantly larger, see Fig. 16.

As expected, the dust polarization spectra show a much weaker E excess at subviscous scales than the synchrotron spectra; see Figs. 17 and 18 and compare with Figs. 10 and B5 of the paper.

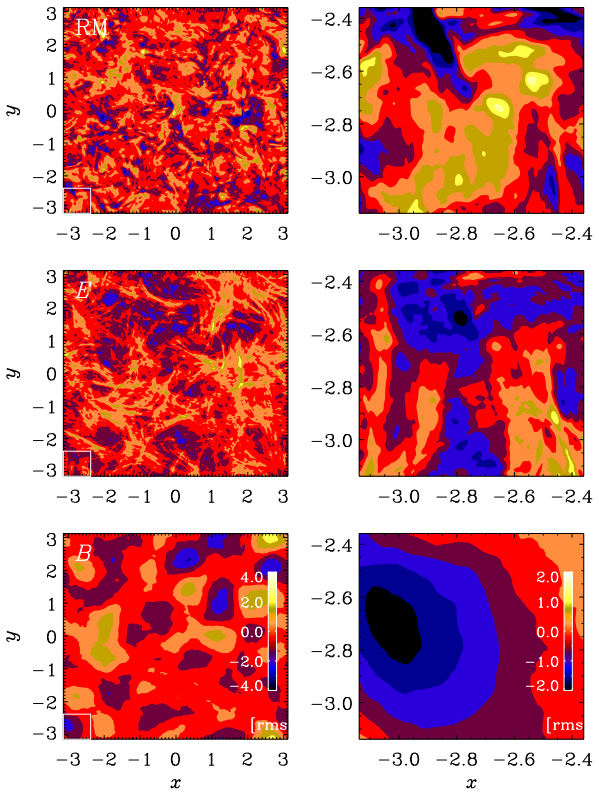

Figure 14: Synchrotron images for Run D (saturated).

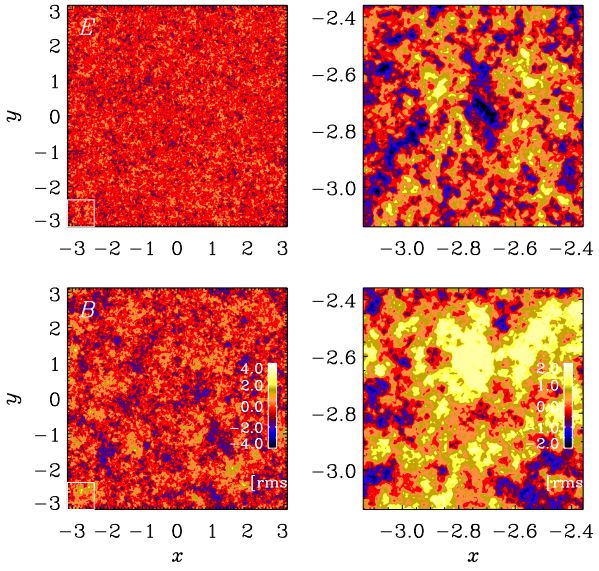

Figure 15: Dust images for Run E (kinematic).

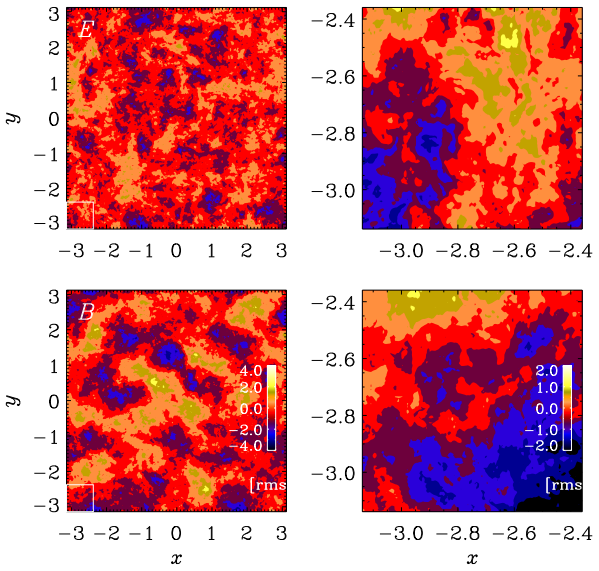

Figure 16: Dust images for Run E (saturated).

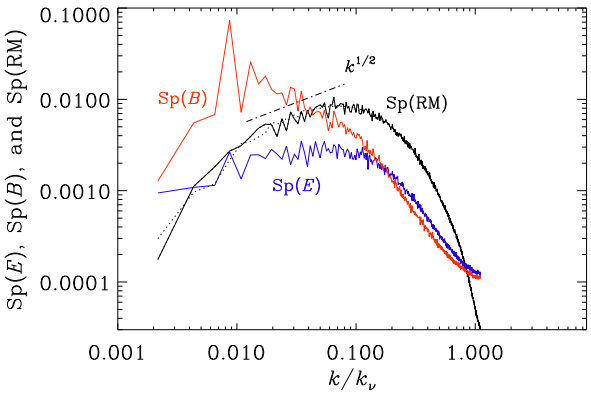

Figure 17: Dust spectra for Run E (kinematic).

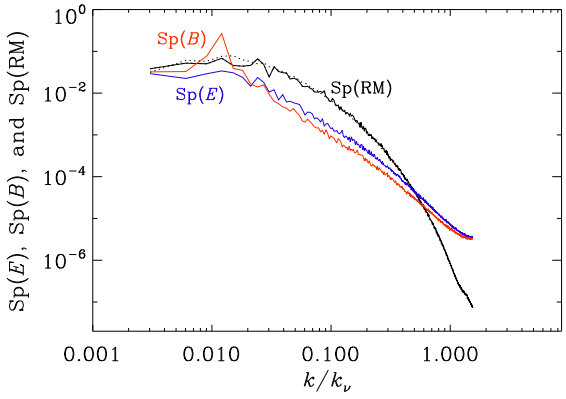

Figure 18: Dust spectra for Run E (saturated).

6.1 Inertial-range dynamo action

Run E has demonstrated that the Kazantsev spectrum extends well into the inertial range to length scales above the viscous scale. Is this truly caused by dynamo action in the inertial range or, perhaps, a nonlocal artifact caused by the strong spike in kinetic energy at the driving scale? As explained

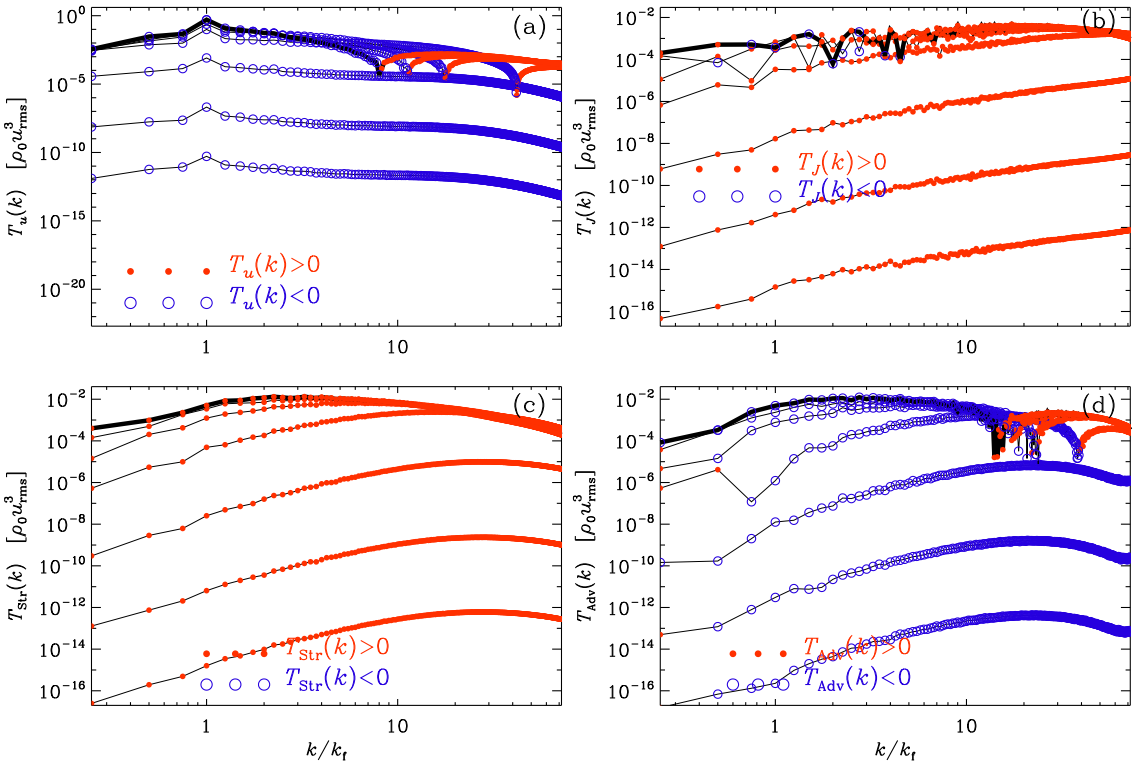

Figure 19: (a) $E_{\rm K}(k)$ (blue dashed) and $E_{\rm M}(k)$ (red solid lines) showing the saturation of the dynamo at eight different times for Run E. (b) The corresponding $T_u(k)$, (c) $T_{\rm Str}$, and (d) $T_{\rm Adv}$ with filled red (open blue) symbols denoting positive (negative) values.

above, those peaks can be very large for large values of $k_{\rm f}/k_1$, although for Run E, this spike is no longer so pronounced. To analyze the spectral energy flux, we follow the procedure of Rempel (2014) and Brandenburg & Rempel (2019) and compute the spectral works done by the Lorentz force and the electromotive force,

$$T_u(k) = {\rm Re}\sum_{k_-<|\boldsymbol{k}|\le k_+} \widetilde{\boldsymbol{u}}_{\boldsymbol{k}} \cdot (\widetilde{\boldsymbol{J}\times\boldsymbol{B}})^*_{\boldsymbol{k}}, \quad (1)$$

$$T_J(k) = {\rm Re}\sum_{k_-<|\boldsymbol{k}|\le k_+} \widetilde{\boldsymbol{J}}_{\boldsymbol{k}} \cdot (\widetilde{\boldsymbol{u}\times\boldsymbol{B}})^*_{\boldsymbol{k}}, \quad (2)$$

where $k_\pm = k \pm \delta k/2$, $\delta k = 2\pi/L$ is the wavenumber increment and also the smallest wavenumber $k_1 \equiv \delta k$ in the domain of side length L, and tildes denote Fourier transformation. The latter can be further decomposed into a contributions from stretching and advection; see Eqs. (4) and (5) of Brandenburg & Rempel (2019).

We see from Fig. 19 that, in the kinematic regime, the work done by the Lorentz force is negative at all wavenumbers and the work done by the electromotive force is positive. Thus, kinetic energy is transferred to magnetic energy at all wavenumbers. In the nonlinear regime, however, there can be reversed dynamo action at small scales, where are magnetic fields drive fluid motions. From Fig. 8, we see that this is mostly caused by advection rather than by stretching. These results are similar to those of Brandenburg & Rempel (2019) for ${\rm Pr_M} \gg 1$ (they used ${\rm Pr_M} = 20$). We can now also conclude that the dynamo works in the entire inertial range, giving thus justification for the occurrence of the Kazantsev spectrum in the entire inertia range.

7 Diagnostics for Run T1

Run T1 employs a non-isothermal two-phase flow, similar to Run T0, but with a helical forcing. In figures 20 and 21 we present its synchrotron images and polarization spectra, respectively. The results are broadly similar to those of Run T0, as well as their single-flow counterpart Run D.

References

Brandenburg, A., & Rempel, M., Reversed dynamo at small scales and large magnetic Prandtl number. *Astrophys. J.* 2019, **879**, 57.

Rempel, M., Numerical simulations of quiet sun magnetism: on the contribution from a small-scale dynamo. *Astrophys. J.* 2014, **789**, 132.

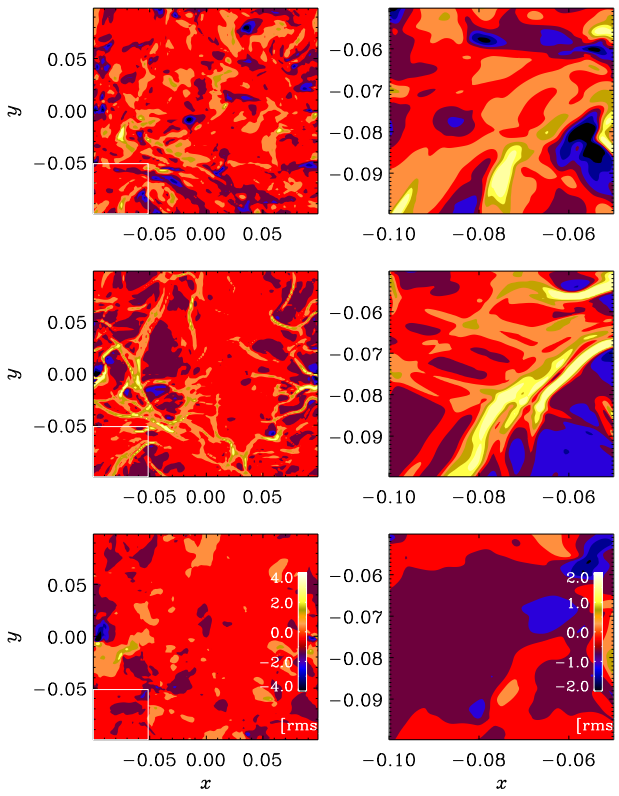

Figure 20: Synchrotron images for Run T1 (kinematic).

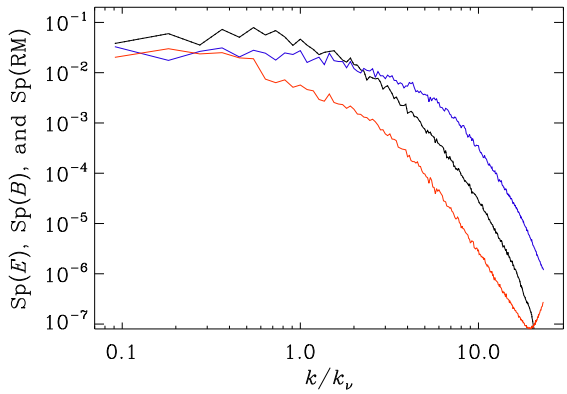

Figure 21: Synchrotron spectra for Run T1 (kinematic).